

Relativistic baryonic jets from an ultraluminous supersoft X-ray source

Ji-Feng Liu¹, Yu Bai¹, Song Wang¹, Stephen Justham¹, You-Jun Lu¹, Wei-Min Gu², Qing-Zhong Liu³, Rosanne Di Stefano⁴, Jin-Cheng Guo¹, Antonio Cabrera-Lavers^{5,6}, Pedro Álvarez^{5,6}, Yi Cao⁷, Shri Kulkarni⁷,

¹*Key Laboratory of Optical Astronomy, National Astronomical Observatories, Chinese Academy of Sciences, 20A Datun Rd, Chaoyang District, Beijing, China 100012*

²*Department of Astronomy, Xiamen University, Xiamen, Fujian Province, China 361005*

³*Key Laboratory of Dark Matter and Space Astronomy, Purple Mountain Observatory, Chinese Academy of Sciences, Nanjing, Jiangsu Province, China 210008*

⁴*Harvard-Smithsonian Center for Astrophysics, Cambridge, MA, USA 02138*

⁵*Instituto de Astrofísica de Canarias, c/Vía Láctea s/n, E-38200 La Laguna, Tenerife, Spain.*

⁶*Departamento de Astrofísica, Universidad de la Laguna, E-38205 La Laguna, Tenerife, Spain.*

⁷*Department of Astronomy, Caltech, Pasadena, CA, USA 91125*

The formation of relativistic jets by an accreting compact object is one of the fundamental mysteries of astrophysics. While the theory is poorly understood, observations of relativistic jets from systems known as microquasars^{1,2} have led to a well-established phenomenology^{3,4}. Relativistic jets are not expected from sources with soft or supersoft X-ray spectra, although two such systems are known to produce relatively low-velocity bipolar outflows^{5,6}. Here we report optical spectra of an ultraluminous supersoft X-ray source (ULS^{7,8}) in the nearby

galaxy M81 (M81 ULS-1^{9,10}) showing blueshifted broad H $_{\alpha}$ emission lines, characteristic of baryonic jets with relativistic speeds. The time variable jets have projected velocities ~ 17 per cent of the speed of light, and seem similar to those in the prototype microquasar SS 433^{11,12}. Such relativistic jets are not expected to be launched from white dwarfs¹³, but an origin from a black hole or neutron star in M81 ULS-1 is hard to reconcile with its constant soft X-rays¹⁰. The completely unexpected presence of relativistic jets in a ULS challenges the canonical theories for jet formation^{3,4}, but may possibly be explained by a long speculated super-critically accreting black hole with optically thick outflows^{14–20}.

Initial spectroscopic observations of M81 ULS-1 made at the Keck Observatory in 2010 found²¹ broad Balmer emission lines (as wide as 400 km/s) on top of a power-law like blue continuum. A very broad emission line (as wide as 30Å, corresponding to 2000 km/s) was detected around 5532/5543Å in both observations, but was not identified with any known spectral lines. We followed up with new spectra obtained at the *Gran Telescopio Canarias* (GTC) in 2015, which again showed the Balmer emission lines and the blue continuum, but the previously-unidentified broad emission line was now at a significantly changed wavelength of 5648Å (Figure 1). This change in observer-frame wavelength immediately suggests that the previously unidentified emission line is a blue-shifted H $_{\alpha}$ emission line emitted by an approaching baryonic relativistic jet, at projected velocities of $-0.17c$. More subsequent follow-up spectra reveal ongoing changes in the projected velocity of the blue-shifted jet, for which we suggest that the best explanation is jet precession, as observed in the prototype microquasar SS 433.

SS 433 has exhibited time-variable blueshift and redshift of optical emission lines emitted by its precessing jets, the long-term monitoring of which has revealed^{11,12} a precession period of 164 days, and an intrinsic jet velocity of $0.26c$. M81 ULS-1 is only the second microquasar identified through directly measuring the blueshift of H_{α} emission lines emitted by its baryonic jets. Other known microquasars^{1,2} have mostly been identified through direct imaging of their radio jets or by interpreting strong non-thermal radio emission as arising from their relativistic jets with velocities above $0.1c$. M81 ULS-1 has not previously been detected by radio surveys, but this is not surprising given the great distance to M81. Were SS 433 placed in M81, its radio flux at Earth would be about $1\mu\text{Jy}$, below the detection sensitivity of current radio facilities, but achievable in the future with the Square Kilometer Array²².

From its X-ray properties¹⁰, M81 ULS-1 is a truly unique jet source, in distinct contrast to all other known microquasars^{1,2}. During all observations of M81 by the Chandra X-ray Observatory since its launch, ULS-1 is always detected and exhibits high and low flux states with count rates ranging from 1 to 70 photons per kilo-second. When in high flux states, M81 ULS-1 clearly exhibits supersoft spectra with blackbody temperatures of 65-100 eV and bolometric luminosities above $10^{39} \text{ erg s}^{-1}$. Somewhat surprisingly, the low flux state of M81 ULS-1 appears as supersoft as the high flux state, with more than 95% of the photons below 1 keV (Figure 2). In contrast, all known microquasars^{1,2} are low-mass or high-mass X-ray binaries, each measured or thought to contain a neutron star or black hole, emitting abundant hard photons above 1 keV. As shown in Fig 2, only a few percent to 35% of their photons are below 1 keV in Chandra observations.

Luminous supersoft sources²³ (SSSs) have supersoft X-ray spectra, and those with luminosities below the Eddington limit for a solar-mass object are conventionally interpreted as white dwarfs accreting at a rate of about $10^{-7} - 10^{-6} M_{\odot} \text{ yr}^{-1}$, for which hydrogen fusion within the accreted material proceeds steadily^{24,25}, but the presence of relativistic jets suggests otherwise in M81 ULS-1. The relativistic jets observed in ULS-1 are simply not expected for typical white dwarfs¹³. Indeed, while low velocity bipolar outflows of a few thousand km s^{-1} are possible and have been observed in SSSs such as RX J0513.9-6951⁵ and RX J0019.8+2156⁶, no relativistic jets have ever been observed from SSSs other than M81 ULS-1. These considerations suggest that the accreting object in M81 ULS-1 is not a white dwarf, adding strong evidence to the idea^{26,27} that SSSs, especially the ultraluminous ones, do not necessarily contain accreting white dwarfs.

If the central engine of M81 ULS-1 is indeed a neutron star or black hole as in all other known microquasars, established phenomenology^{3,4} expects steady jets to be generated in the low-hard state, with episodic jets generated in the very high state or during the state transitions between soft and hard states. In the case of M81 ULS-1, the blue-shifted H_{α} emission lines emitted from the relativistic jets were present in all six optical spectroscopic observations in 2010 and 2015. Standard presumptions would therefore be that M81 ULS-1 is in the low-hard or very high states for a substantial fraction of the time, during which abundant hard photons above 1 keV are expected as in other microquasars (Fig 2). Contrary to the above expectations, ULS-1 has been persistently supersoft in all 19 Chandra observations, regardless of whether it is displaying a low or high flux state, suggesting that its relativistic jets are not generated in the canonical ways. In fact, the persistently supersoft appearance of ULS-1 is not expected in any spectral states in the

standard accretion scenarios^{28,29} for neutron star or black hole X-ray binaries, which are known to be accreting below the critical (i.e., Eddington) rate.

This unusual combination of relativistic jets and persistently supersoft X-ray spectra is completely unexpected, posing challenges to our conventional understanding of jet formation^{3,4}. One possible explanation for M81 ULS-1 can be a long speculated^{14,15} super-critically accreting black hole with optically thick outflows. Recent magneto-hydrodynamic simulations of such systems, although still under development and in heated debate^{16,17}, can generate super-Eddington luminosities, and necessarily³⁰ generate disk winds and funnels along the rotation axis, from which radiation pressure will drive baryon-loaded relativistic jets with velocities up to $0.3c$ regardless the black hole spin¹⁷. M81 ULS-1 qualitatively matches both predictions of high luminosities and baryon-loaded relativistic jets, and its supersoft X-ray spectra can potentially be expected from optically thick outflows for suitable outflow geometry, wind velocities and outflow mass rates¹⁸⁻²⁰. Thus, ULS-1 may potentially be a vivid manifestation of recent predictions for super-critical accretion onto black holes, and so reveal the nature of extreme accretion in extreme conditions.

1. Mirabel, I.F., Rodriguez, L.F. Microquasars in our Galaxy. *Nature* **392**, 673-676 (1998)
2. Paredes, J.M., Marti, J. Microquasars in the Galaxy. *Contributions to Science*, **2**, 303-314 (2003)
3. Fender, R. P., Belloni, T. M., & Gallo, E. Towards a unified model for black hole X-ray binary jets. *Mon. Not. R. Astron. Soc.* **355**, 1105-1118 (2004)
4. Migliari, A. & Fender, R.P. Jets in neutron star X-ray binaries: a comparison with black holes.

- Mon. Not. R. Astron. Soc.* **366**, 79-91 (2006)
5. Southwell, K. A., Livio, M., Charles, P. A., O'Donoghue, D., & Sutherland, W. J. The Nature of the Supersoft X-Ray Source RX J0513-69. *Astrophys. J.* **470**, 1065-1074 (1996)
 6. Becker, C. M., Remillard, R. A., Rappaport, S. A., & McClintock, J. E. Bipolar Jets and Orbital Dynamics of the Supersoft X-Ray Source RX J0019.8+2156. *Astrophys. J.* **506**, 880-891 (1998)
 7. Di Stefano, R. & Kong, A.K.H. Luminous Supersoft X-Ray Sources in External Galaxies. *Astrophys. J.* **592**, 884-899 (2003)
 8. Swartz, D. A., Ghosh, K. K., Suleimanov, V., Tennant, A. F., Wu, K. Chandra Discovery of Luminous Supersoft X-Ray Sources in M81. *Astrophys. J.* **574**, 382-397 (2002)
 9. Liu, J.-F. & Di Stefano, R. An Ultraluminous Supersoft X-Ray Source in M81: An Intermediate-Mass Black Hole? *Astrophys. J.* **674**, L73-L76 (2008)
 10. Liu, J.-F. No Periodicity Revealed for an "Eclipsing" Ultraluminous Supersoft X-Ray Source in M81. *Astrophys. J. Suppl. Ser.* **177**, 181-188 (2008)
 11. Margon, B. Observations of SS 433. *Annu. Rev. Astron. Astrophys.* **22**, 507-536 (1984)
 12. Blundell, K. M., Bowler, M. G., Schmidtbreick, L. Fluctuations and symmetry in the speed and direction of the jets of SS 433 on different timescales. *Astron. Astrophys.* **474**, 903-910 (2007)
 13. Livio, M. Astrophysical Jets. *Probing the Physics of Active Galactic Nuclei* **224**, 225 (2001)

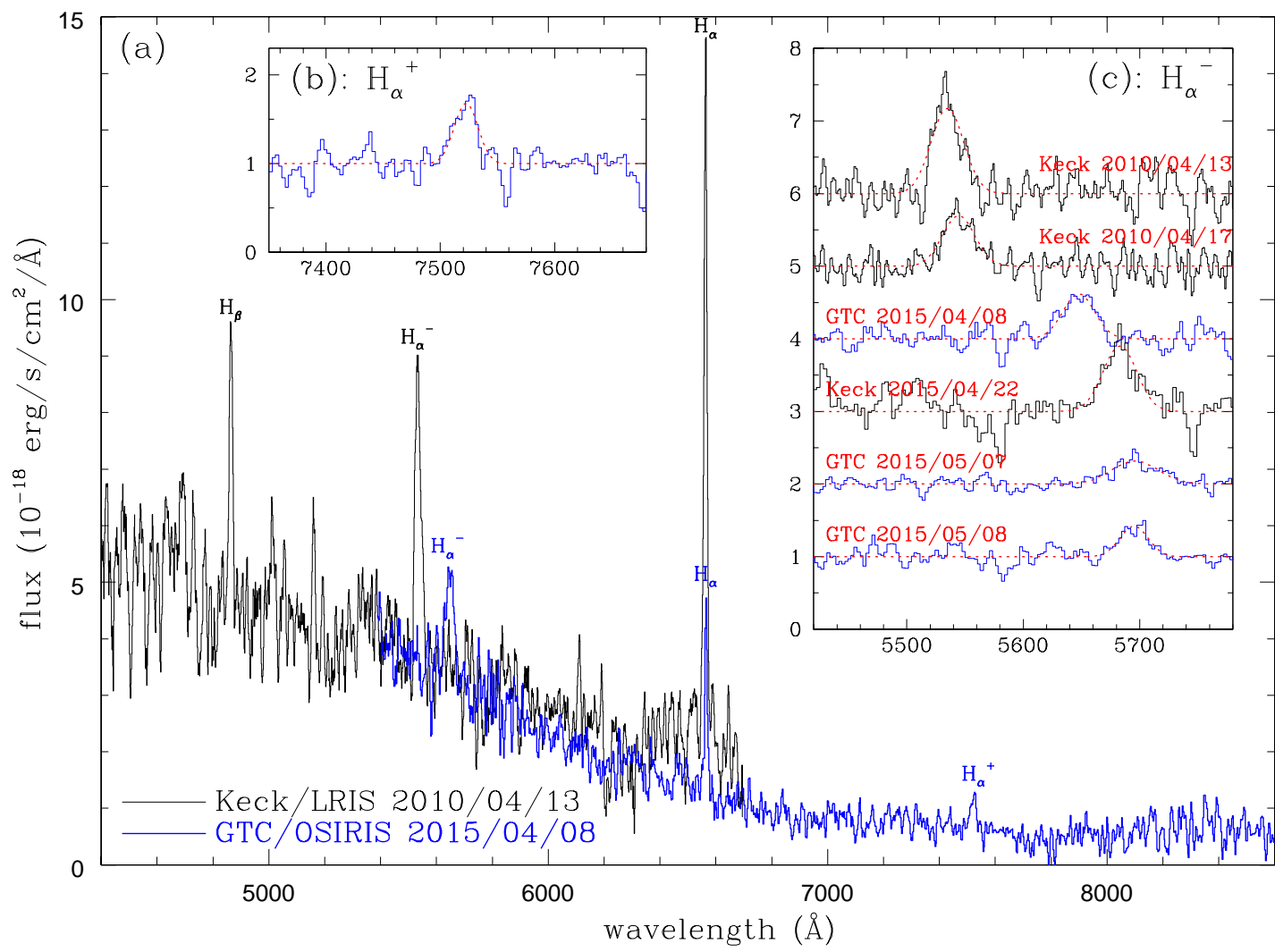
14. Paczyński, B., & Wiita, P.J. Thick accretion disks and supercritical luminosities. *Astron. Astrophys.* **88**, 23-31 (1980)
15. Abramowicz, M.A., Czerny, B., Lasota, J.P., & Szuszkiewicz, E. Slim accretion disks. *Astrophys. J.* **332**, 646-658 (1988)
16. Jiang, Y.-F., Stone, J.M., & Davis, S.W. A Global Three-dimensional Radiation Magneto-hydrodynamic Simulation of Super-Eddington Accretion Disks. *Astrophys. J.* **796**, 106 (2014)
17. Sadowski, A. & Narayan, R. Powerful radiative jets in super-critical accretion disks around non-spinning black holes. *arXiv:1503.00654* (2015)
18. Ohsuga, K., Mori, M., Nakamoto, T. & Mineshige, S. Supercritical Accretion Flows around Black Holes: Two-dimensional, Radiation Pressure-dominated Disks with Photon Trapping. *Astrophys. J.* **628**, 368-381 (2005)
19. King, A. & Pounds, K. Black hole winds. *Mon. Not. R. Astron. Soc.* **345**, 657-659 (2003)
20. Shen, R.-F., Duran, R.B., Nakar, E. & Piran, T. The nature of ULX source M101 ULX-1: optically thick outflow from a stellar mass black hole. *Mon. Not. R. Astron. Soc.* **447**, L60-L64 (2015)
21. Bai, Y., Liu, J., & Wang, S. Spectroscopic Studies of an Ultraluminous Supersoft X-Ray Source in M81. *Astrophys. J.* **802**, L27 (2015)

22. R. T. Schilizzi, R.T.; Alexander, P.; Cordes, J.M. et al. Preliminary specifications for the SKA, https://www.skatelescope.org/uploaded/5110_100_Memo_Schilizzi.pdf (2007)
23. Kahabka, P. & van den Heuvel, E. P. J. Luminous Supersoft X-Ray Sources. *Annu. Rev. Astron. Astrophys.* **35**, 69-100 (1997)
24. Iben, I., Jr. Hot accreting white dwarfs in the quasi-static approximation. *Astrophys. J.* **259**, 244-266 (1982)
25. Nomoto, K. Accreting white dwarf models for type I supernovae. I - Presupernova evolution and triggering mechanisms. *Astrophys. J.* **253**, 798-810 (1982)
26. Di Stefano, R. & Kong, A. The Discovery of Quasi-soft and Supersoft Sources in External Galaxies. *Astrophys. J.* **609**, 710-727 (2004)
27. Di Stefano, R.; Primini, F.A.; Liu, J.-F.; Kong, A. & Patel, B. Populations of supersoft X-ray sources: Novae, tidal disruption, Type Ia supernovae, accretion-induced collapse, ionization, and intermediate-mass black holes? *Astronomische Nachrichten*, **331**, 205-211 (2010)
28. Remillard, R. A. & McClintock, J. E. X-ray properties of black-hole binaries. *Annu. Rev. Astron. Astrophys.* **44**, 49-92 (2006)
29. Hasinger, G. & van der Klis, M. Two patterns of correlated X-ray timing and spectral behaviour in low-mass X-ray binaries. *Astron. Astrophys.* **225**, 79-96 (1989)
30. Gu, W.-M. Mechanism of Outflows in Accretion System: Advective Cooling cannot Balance Viscous Heating? *Astrophys. J.* **799**, 71 (2015)

Acknowledgements We thank Drs Katherine Blundell, Ramesh Narayan, Zhiyuan Li, Tinggui Wang, Feng Yuan, Xuan Fang, Jimmy Irwin, Tom Maccarone and Doug Swartz for helpful discussions. Authors acknowledge supports from the Chinese Academy of Sciences through Grant No. XDB09000000, from 973 Program 2014CB845705, and from National Science Foundation of China through grants NSFC-11333004/11425313. This work is partly based on observations made with the Gran Telescopio Canarias (GTC), installed in the Spanish Observatorio del Roque de los Muchachos of the Instituto de Astrofísica de Canarias, in the island of La Palma. Part of the data was obtained at the W.M. Keck Observatory, which is operated as a scientific partnership among the California Institute of Technology, the University of California and the National Aeronautics and Space Administration. The Observatory was made possible by the generous financial support of the W.M. Keck Foundation.

Author contributions J.-F.L. proposed the observations. J.-F.L., Y.B. and S.W. reduced the optical and X-ray data and carried out the analysis. J.-F.L., S.J., Y.-J.L. and R.D.S. discussed the results and drafted the manuscript. All authors commented on and helped improving the manuscript.

Author information Reprints and permissions information is available at npg.nature.com/reprints. The authors declare that they have no competing financial interests. Readers are welcome to comment on the online version of the paper. Correspondence and requests for materials should be addressed to J.F. Liu (email: jfliu@nao.cas.cn).



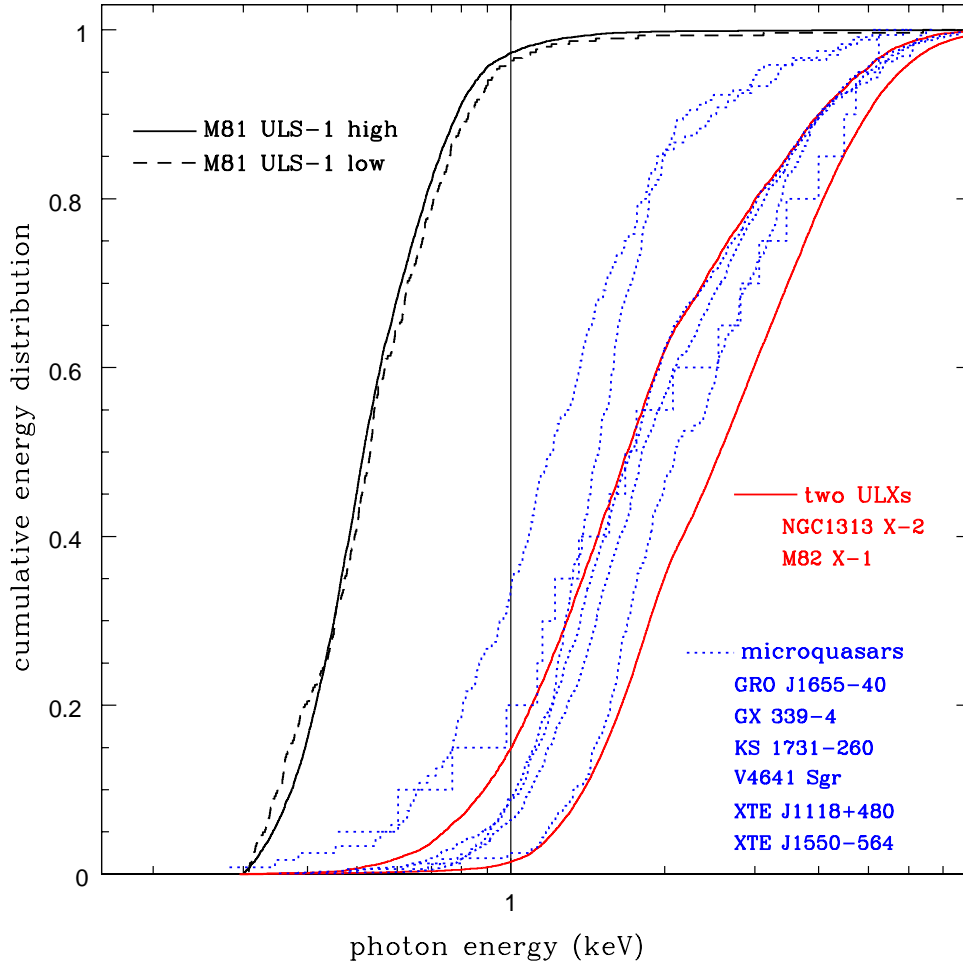


Figure legends

Figure 1. Keck and GTC spectra for the optical counterpart of M81 ULS-1. (a) The Keck/LRIS spectrum taken on 2010/04/13 (blue channel; black) and the GTC/OSIRIS spectrum taken on 2015/04/08 (red) for M81 ULS-1. Labeled over the lines are the broad Balmer lines (H_α and H_β), the very broad blue-shifted H_α^- at 5530\AA and 5648\AA . The power-law like continuum and the broad Balmer lines are characteristic of an accretion disk around a compact object, which confirms the physical association between the X-ray source and its optical counterpart. (b) The blue-shifted

H_{α}^{-} from six Keck and GTC observations with time-variable observer-frame central wavelengths. The intensities also change with time in proportion to the intensities of the stationary H_{α} emission line from the accretion disk, suggesting a link between the accretion and the jet. See the Methods for details. Both the spectra and the fits are normalized by the underlying continuum, and are shifted vertically for clarity.

Figure 2. Cumulative photon energy distributions for M81 ULS-1. Also plotted for comparison are two typical ultraluminous X-ray sources in nearby galaxies (ULXs; M82 X-1 and NGC1313 X-2), and six Galactic microquasars observed with ACIS aboard the Chandra X-ray Observatory. Most photons concentrate at energies where the cumulative distribution rises fastest. For M81 ULS-1, there are more than 95% of the photons below 1 keV both in the low state (black solid) and the high state (red solid). There are less than 15% of the photons below 1 keV for both ULXs (red solid). For all six Galactic microquasars (blue dotted), there are only a few percent to less than 35% of the photons below 1 keV. Since the response matrix is not well calibrated below 0.3 keV for Chandra/ACIS, only photons above 0.3 keV are used for the above sources.

Methods

GTC/OSIRIS and Keck/LRIS data reduction Initial optical spectroscopic observations of M81 ULS-1 were carried out with Keck/LRIS on 2010 April 13 and 17, which revealed broad Balmer emission lines as from an accretion disk²¹. The emission line of the blue-shifted H_{α} (H_{α}^{-}) is shown at 5530 Å in the spectra, with a shift in the line centre of $10 \text{ \AA} \pm 2 \text{ \AA}$ between those

two observations (i.e., two epochs separated by four nights).

M81 ULS-1 was later observed using GTC/OSIRIS on 2015 April 8, May 7 and 8, masked with the 0.6'' slit followed by the R1000R grating, which yields a resolution of about 7 Å. The spectra were reduced in a standard way with IRAF. After bias subtraction and flat correction, the dispersion correction was carried out based on the line lists given in the OSIRIS manual (see <http://www.gtc.iac.es/instruments/osiris/>). Raw spectra were then extracted with an aperture size of 1'', and a standard star taken at each night was used to make the flux calibration.

On 2015 April 22, another observation of M81 ULS-1 was carried out using Keck/LRIS with the 1.0'' slit. The light was split with a beam dichroic of 6800 Å to the blue and red sides followed by the 300/5000 and 400/8500 gratings, which yields a resolution of ~ 8 Å. The spectrum was reduced with the IDL pipeline designed for Keck.

Extended Data Table 1 lists the basic information of the observations from 2010 to 2015. Both H_{α} and H_{α}^{-} emission lines are detected in all the spectra, and their line properties are calculated from Gaussian line profile fitting. Extended Data Table 2 lists the central wavelength, the full width at half-maximum (FWHM) and the equivalent width (E.W.) for each fitted emission line. The observed H_{α}^{-} central wavelengths λ_{-} correspond to projected velocities v_r from $-0.17c$ to $-0.14c$ in these observations given $\lambda_{-}/\lambda_0 = \sqrt{\frac{1+v_r/c}{1-v_r/c}}$.

Properties of the emission lines In the case of SS433, the E.W.s of H_{α} are tightly correlated with the phases of the precession, and those of the H_{α}^{-} emission follow a similar trend but with a phase delay³¹. We use the power of the emission lines, calculated from the area of the Gaussian

fitting, as representative of the emission intensity, since the observed continuum from M81 ULS-1 varies significantly between observations. Extended Data Figure 1 shows that the power of H_{α} emission lines from the accretion disk is positively correlated with that of the H_{α}^{-} emission lines, suggesting a link between the accretion and the jet. The variations of the emission-lines' power are asymmetrical with smooth rises and steeper declines around 2015 May 7 (Extended Data Figure 2), which are similar to those of SS433³¹.

The rate at which the projected H_{α}^{-} velocity changes appears slower during the observations in 2015 compared to those in 2010. The rate of change in 2015 is roughly 0.8 \AA day^{-1} , whereas it was 2.6 \AA day^{-1} in 2010; if the velocity shift is due to precession this may naturally be explained because the 2015 observations are sampling a different part of the precession cycle. We can estimate a minimum likely precession period by assuming that the turning point of the precession cycle occurred around the observations of May 7 and 8, 2015 (see Extended Data Figures 2 and 3). In that case then, after the wavelength of the emission lines reached the maximum in May 8 (Extended Data Figure 2), the H_{α}^{-} emission likely turned back to the short wavelength with the rate of roughly $-0.8 \text{ \AA day}^{-1}$, indicating that the half precession period must be longer than 30 days. There is a 115 \AA gap between the observations in 2010 April 13 and 2015 April 08 (Extended Data Figure 3), and if we assume that the maximum rate at which the wavelength decreases is 2.6 \AA day^{-1} , the line H_{α}^{-} needs 44 days to move by the required amount. Therefore, the half precession period is likely longer than 74 days, and lower limit of the precession period is about 148 days. More time resolved spectra are needed in order to derive an accurate period and further characterize the apparent precession of the jets.

Searching for the red-shifted H_α emission lines Given the blueshifted H_α^- emission lines from the approaching jets, the redshifted H_α emission lines (H_α^+) are expected from the receding jets, albeit with much lower intensities due to Doppler boosting effects. Assuming symmetrical and steady jets, the boosting factors for the lines emitted from the approaching and the receding jets are given by $\mathcal{D}_- = \frac{(1-\beta^2)^{1/2}}{1-\beta \cos \theta} > 1$, and $\mathcal{D}_+ = \frac{(1-\beta^2)^{1/2}}{1+\beta \cos \theta} < 1$, respectively. The total flux of a blue- or red-shifted line in the observer frame is boosted by a factor of D^3 . The expected central wavelengths of the two lines are $\lambda_- = \lambda_0/\mathcal{D}_-$, and $\lambda_+ = \lambda_0/\mathcal{D}_+$, and the corresponding redshifts are $z_+ = \lambda_+/\lambda_0 - 1 > 0$ and $z_- = \lambda_-/\lambda_0 - 1 < 0$. Both D and z for H_α^- in all observations are listed in Extended Data Table 3.

We have searched for the redshifted H_α^+ in all observations. A weak emission line feature was detected at $\sim 3\sigma$ around 7524\AA (see Figure 1), roughly symmetrical to H_α^- at 5648\AA , in one of the GTC exposure during the night of April 08, 2015. If this marginal detection were the red-shifted H_α^+ , its boosting factor is $\mathcal{D}_+ = \lambda_0/\lambda_+ = 0.8722$, the ratio of the received total flux of the blue shift line to that of the the redshift line should be $D_-^3/D_+^3 \sim 2.5$, which is roughly consistent with the observational one ($\sim 4_{-1.5}^{+3.5}$).

However, the observed wavelength is not consistent with the expected H_α^+ wavelength given the blueshifted H_α^- at 5648\AA , i.e., $5648 = 6563 \left[\frac{1-\beta \cos \theta}{(1-\beta^2)^{1/2}} \right]$. Assuming the extreme case, $\theta = 0^\circ$, then we have $\beta = 0.1491$. If the receding jet has the same velocity, then the expected central wavelength of H_α^+ should be 7626.4\AA , which is about 104\AA larger than the detected line. If assuming $\theta = 10^\circ/20^\circ/30^\circ$, then $\beta = 0.152/0.160/0.177$ and then the expected central wavelength of H_α^+ is $7632/7650/7688\text{\AA}$, which is about $108/126/164\text{\AA}$ larger than the detected line. The

discrepancy becomes larger for larger inclination angles.

This casts doubt on the identification of the 7524Å line feature as H_{α}^{+} , unless the jets are asymmetrical or fast changing. We may have not detected the redshifted H_{α}^{+} , but the non-detection is not surprising given the Doppler boosting effects, and other realistic reasons. For example, the receding jets may be blocked by the optically thick outflows if this system is a super-critically accreting black hole system as described in the manuscript. No candidate H_{α}^{+} emission lines were detected at all in the May 7 and 8 GTC observations, or in the Keck spectrum. Even if the April 8 line were a true H_{α}^{+} emission line, this non-detection would not be surprising, given the lower E.W.s of H_{α}^{-} on May 7 and 8, and the relatively lower sensitivity in the red channel of LRIS.

Analysis of *Chandra* data There have been 19 *Chandra*/ACIS observations of the nuclear region of M81, where ULS-1 resides. All of these observations were derived from the *Chandra* archive and analyzed uniformly with the CIAO 4.7 software tools. Point sources were detected with WAVDETECT on the individual *Chandra* images. As listed in Extended Data Table 4, the photon counts were extracted from the source ellipses enclosing 95% of the total photons as reported by WAVDETECT, which was run with scales of 1'', 2'', 4'', and 8'' in the 0.3–8.0 keV band.

The spectra in the high states (Count Rate > 10 count ks⁻¹) were fitted by absorbed blackbody models, with the spectral parameters presented in Extended Data Table 4, all of which show that M81 ULS-1 has been persistently supersoft in these observations. In addition, the spectra in high and low states were co-added into combined high- and low-state spectra, and were also fitted in the band of 0.3–8.0 keV. Using the fitted absorbed blackbody model, we calculated the 0.3–8.0 keV

flux, the 0.3–8.0 keV luminosity and the bolometric luminosity with the distance of 3.63 Mpc for M81³².

As plotted in Extended Data Figure 4, M81 ULS-1 displays a soft excess below 0.3 keV as compared to the best-fit model for 0.3-8.0 keV. However, considering that the response matrix for *Chandra* is not well calibrated below 0.3 keV, we refrain from interpreting this soft excess. Nonetheless, it is clear that M81 ULS-1 has very different spectral properties from the other known microquasars. Moreover, these uncertainties in calibration below 0.3 keV only have the potential for the intrinsic spectral differences between M81 ULS-1 and the other known microquasars to be even larger (i.e., the energy distribution from M81 ULS-1 may be even softer than observed).

Code Availability The optical spectra were reduced with IRAF available at <http://iraf.noao.edu/>. All the emission lines in Extended Data Table 2 were fitted with the curve fitting toolbox based on Matlab (see <http://www.mathworks.com/help/curvefit/index.html>). The *Chandra* archive data were analyzed with CIAO 4.7 which can be downloaded from <http://cxc.harvard.edu/ciao/download/>.

31. Vittone, A., Rusconi, L., Sedmak, G., Mammano, A., Ciatti, F. Correlations and periodicities of equivalent widths in SS 433. *Astron. Astrophys. Suppl. Ser.* **53**, 109-117 (1983)

32. Freedman, W. L., Hughes, S. M., Madore, B. F., et al. The Hubble Space Telescope Extragalactic Distance Scale Key Project. 1: The discovery of Cepheids and a new distance to M81. *The Astrophysical Journal.* **427**, 628-655 (1994)

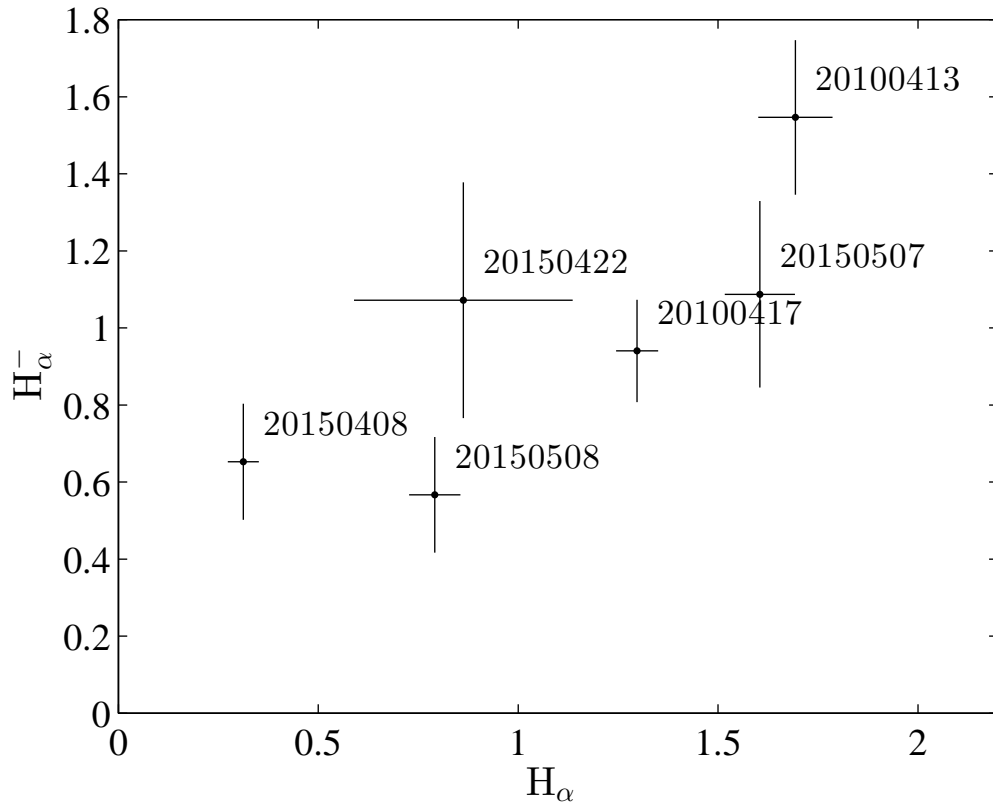
Legends for Extended Data Tables

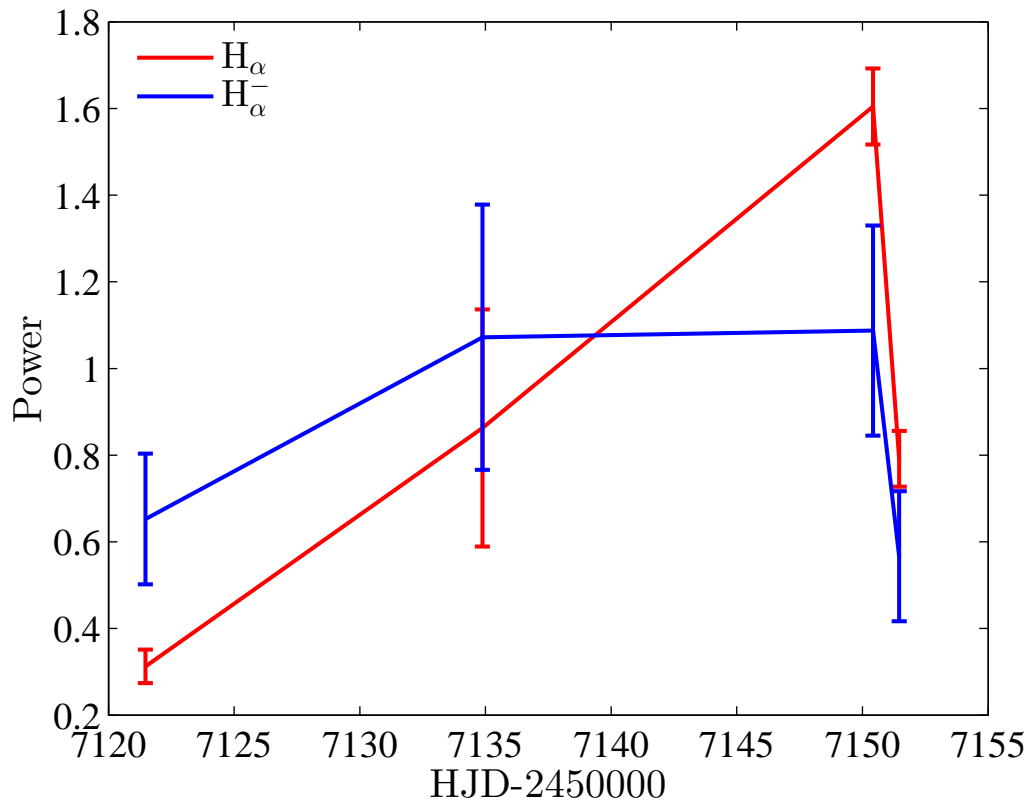
Extended Data Table 1. Observations of M 81 ULS-1. The columns are: (1) observation date, (2) telescope, (3) exposure time. (4) spectral resolution.

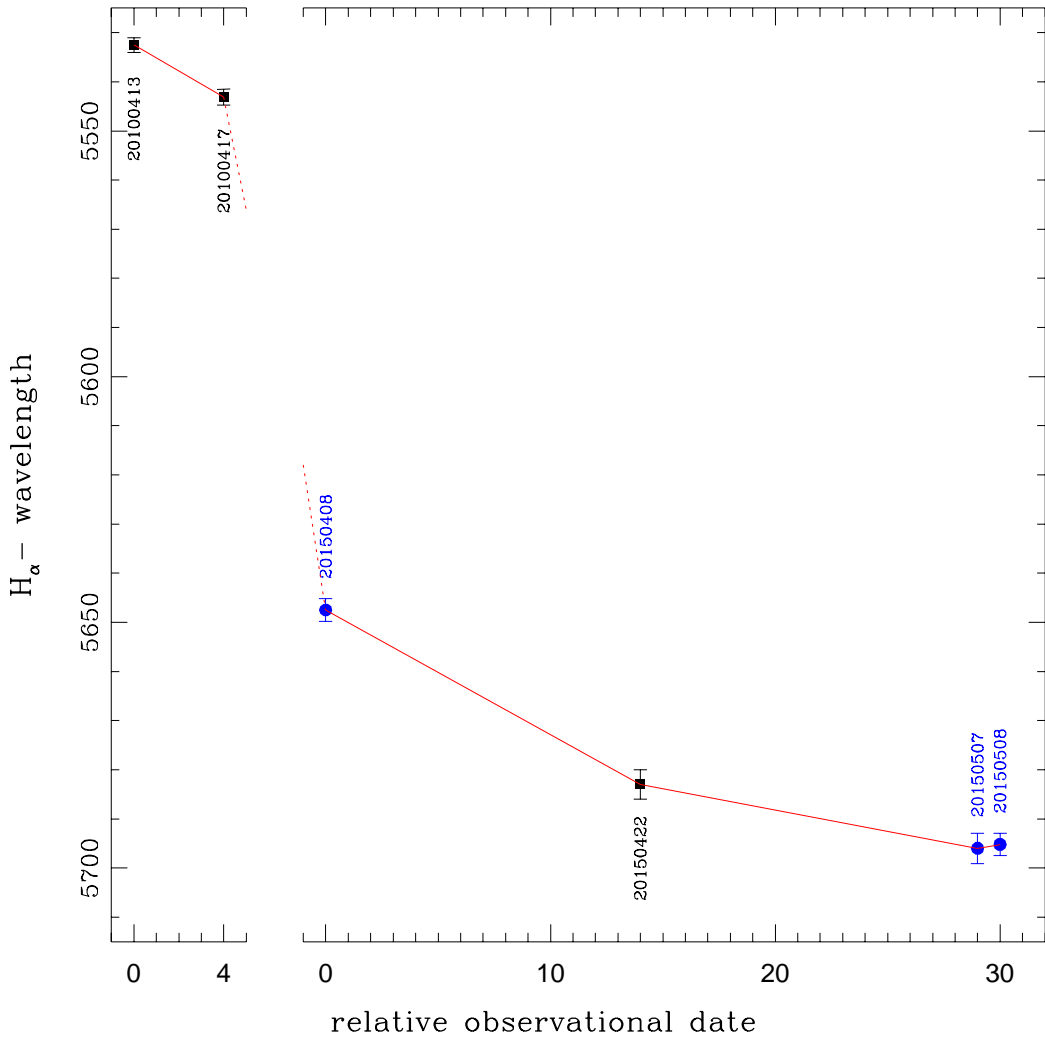
Extended Data Table 2. Properties of H_{α}^{-} , H_{α}^{+} (?) and H_{α} . The center, FWHM and E.W. are in unit of Å. The number given in the bracket is the velocity in unit of the speed of light. The power is in unit of 10^{-16} erg s⁻¹ cm⁻². All the errors refer to 68.3% uncertainties.

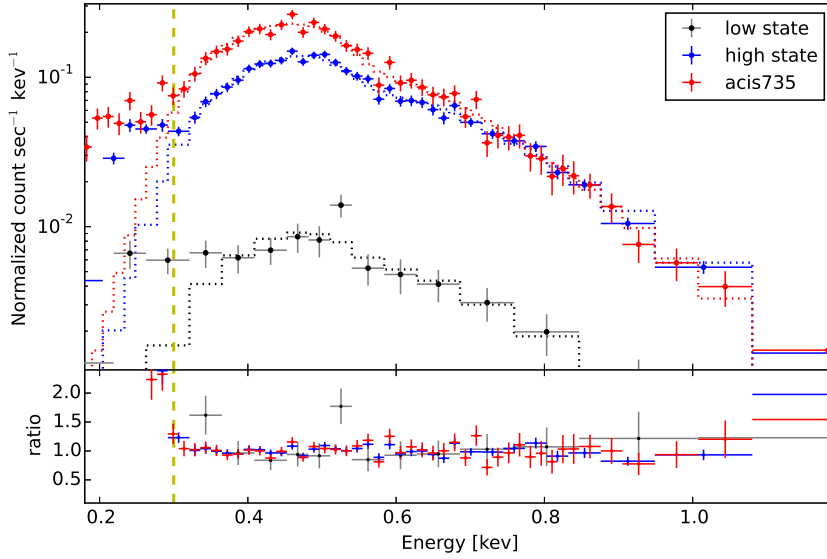
Extended Data Table 3. Doppler boost factors for each observation. The columns are: (1) observation date, (2) wavelength of the blueshifted/redshifted H_{α} , (3) Doppler boosting factor, (4) redshift.

Extended Data Table 4. *Chandra* Observations of M81 ULS-1. NOTES: Col. (1): ObsID. Col. (2): Obs Date. Col. (3): Ontime without deadtime correction. Col. (4): Net counts in 0.1-8.0 keV. Col. (5): Counts in the supersoft band, 0.1-0.5 keV. Col. (6): Count rate after vignetting correction. Col. (7): Temperature for the blackbody fit to the spectrum in 0.3-8.0 keV. Col. (8): Neutral hydrogen column density. Col. (9): The 0.3-8.0 keV flux for the blackbody fit to the spectrum. (10): The 0.3-8.0 keV luminosity. (11): The unabsorbed bolometric luminosity. Col. (12): Reduced χ^2 and degree of freedom for the spectral fit. Col. (13): Flags indicating a high low state, seprated by Count Rate = 10 count ks⁻¹.









Legends for Extended Data Figures

Extended Data Figure 1. The power of H_{α}^{-} vs. that of H_{α} in unit of $10^{-16} \text{ erg s}^{-1} \text{ cm}^{-2}$. The error bars account for the 68.3% uncertainties.

Extended Data Figure 2. The variation of the power of emission lines in unit of $10^{-16} \text{ erg s}^{-1} \text{ cm}^{-2}$. The error bars account for the 68.3% uncertainties.

Extended Data Figure 3. The center of H_{α}^{-} as a function of relative observational date. The dates of observations are marked in the figure. The error bars account for the 68.3% uncertainties.

Extended Data Figure 4. The M81 ULS-1 spectra from ObsID 735. The spectra are combined high-state observations, and combined low-state observations, shown with red, blue, and black crosses, fitted by blackbody model in the 0.3-8.0 keV with red, blue, and black dotted lines. The yellow dashed line indicates photon counts with energy of 0.3 keV. The error bars account for the 68.3% uncertainties.

Table 1:

Date	Telescope	Exposure Time (second)	$\Delta\lambda$ (Å)
2010.4.13	Keck	1000×3	5
2010.4.17	Keck	1200×2	5
2015.4.08	GTC	1800×3	7
2015.4.22	Keck	2800×2	8
2015.5.07	GTC	1800×3	7
2015.5.08	GTC	1800×4	7

Table 2:

HJD-2450000	H_{α}^{-+}			H_{α}			
	Center	FWHM	E.W.	Power	Center	FWHM	Power
5299.83	$5532.3 \pm 1.5 (-0.17c)$	33 ± 4	41 ± 5	1.55 ± 0.20	6562.9 ± 0.2	10.8 ± 0.5	1.69 ± 0.09
5303.77	$5543.1 \pm 1.6 (-0.17c)$	33 ± 4	24 ± 3	0.94 ± 0.13	6562.8 ± 0.2	9.4 ± 0.3	1.30 ± 0.05
7121.47	$5647.5 \pm 2.3 (-0.15c)$	32 ± 6	21 ± 5	0.65 ± 0.15	6564.9 ± 0.3	6.7 ± 0.6	0.31 ± 0.04
7134.88	$5683.0 \pm 3.0 (-0.14c)$	34 ± 7	33 ± 9	1.07 ± 0.31	6564.4 ± 0.9	8.9 ± 2.1	0.86 ± 0.27
7150.42	$5696.0 \pm 3.1 (-0.14c)$	46 ± 8	16 ± 4	1.08 ± 0.24	6564.1 ± 0.1	7.6 ± 0.3	1.60 ± 0.09
7151.46	$5695.2 \pm 2.3 (-0.14c)$	29 ± 6	13 ± 3	0.57 ± 0.15	6564.4 ± 0.2	7.4 ± 0.5	0.79 ± 0.06
7121.47	$7522.1 \pm 2.7 (+0.14c)$	20 ± 6	27 ± 7	0.16 ± 0.05			

Table 3:

Date	$\lambda(\text{H}_\alpha^- \text{ or } \text{H}_\alpha^+?)$	D	z
20100413	5532.5	1.1862	-0.1570
20100417	5543.1	1.1840	-0.1554
20150408	5647.5	1.1621	-0.1395
20150422	5683.0	1.1548	-0.1341
20150507	5696.0	1.1522	-0.1321
20150508	5695.2	1.1523	-0.1322
20150408	7524.0	0.8722	0.1465

Table 4:

ObsID	Obs Date	ExpT (ks)	C_{NET}	C_{Soft}	Count Rate (count ks ⁻¹)	kT_{bb} (eV)	n_{H} (10 ²⁰ cm ⁻²)	Flux (ergs s ⁻¹ cm ⁻¹)	L_X (10 ³⁸ ergs s ⁻¹)	L_{bol} (10 ³⁸ ergs s ⁻¹)	χ^2_{ν}/dof	State
acis390	2000 Mar 21	2.4	140	25	60.81± 5.74	145±40.9	12.5±20.0	1.42e-13	2.3	6.7	1.390/4	high
acis735	2000 May 07	50.7	3679	2141	67.16± 1.19	78±1.6	9.5±1.0	1.99e-13	3.1	23.1	1.086/41	high
acis5935	2005 May 26	11.1	11	2	1.06 ± 0.43							low
acis5936	2005 May 28	11.6	11	2	0.82 ± 0.40							low
acis5937	2005 Jun 01	12.2	22	6	1.63 ± 0.46							low
acis5938	2005 Jun 03	12.0	485	185	37.69± 1.87	81±6.2	12.0±5.8	1.89e-13	3.0	25.6	2.041/17	high
acis5939	2005 Jun 06	12.0	364	181	27.53± 1.61	76±5.6	8.3±4.2	1.62e-13	2.6	17.7	0.857/13	high
acis5940	2005 Jun 09	12.1	70	20	4.90 ± 0.73							low
acis5941	2005 Jun 11	12.0	429	187	32.16± 1.74	91±5.8	6.5±4.0	1.74e-13	2.8	10.6	1.004/17	high
acis5942	2005 Jun 15	12.1	405	206	30.30± 1.68	70±5.4	14.1±5.1	1.68e-13	2.7	42.5	0.724/14	high
acis5943	2005 Jun 18	12.2	525	187	41.30± 1.94	91±5.4	8.8±3.8	2.10e-13	3.3	16.0	1.096/21	high
acis5944	2005 Jun 21	12.0	356	85	28.71± 1.64	96±9.8	20.6±8.6	1.16e-13	1.8	20.3	1.128/15	high
acis5945	2005 Jun 24	11.7	415	220	32.04± 1.75	65±4.4	19.8±5.3	1.69e-13	2.7	97.4	1.028/14	high
acis5946	2005 Jun 26	12.2	287	167	20.75± 1.40	70±7.1	10.6±5.9	1.29e-13	2.0	22.5	1.160/8	high
acis5947	2005 Jun 29	10.8	40	29	2.81 ± 0.62							low
acis5948	2005 Jul 03	12.2	77	51	4.93 ± 0.73							low
acis5949	2005 Jul 06	12.2	54	33	3.36 ± 0.62							low
acis9805	2007 Dec 21	5.2	44	28	7.55 ± 1.43							low
acis9122	2008 Feb 01	10.0	55	18	5.40 ± 0.87							low
Total high		149.3	7085	3584	37.85± 2.53	84±1.3	8.2±0.1	1.98e-13	3.1	16.9	1.739/31	
Total low		97.4	384	189	3.61± 0.81	82±8.3	5.6±11.3	2.03e-14	0.3	1.4	1.069/12	